



McVitie, S., McGrouther, D., McFadzean, S., MacLaren, D. A., O'Shea, K. J., and Benitez Romero, M. J. (2015) Aberration corrected Lorentz scanning transmission electron microscopy. *Ultramicroscopy*, 152, pp. 57-62.

Copyright © 2015 Elsevier B.V.

A copy can be downloaded for personal non-commercial research or study, without prior permission or charge

Content must not be changed in any way or reproduced in any format or medium without the formal permission of the copyright holder(s)

<http://eprints.gla.ac.uk/102200/>

Deposited on: 03 February 2015

Enlighten – Research publications by members of the University of Glasgow
<http://eprints.gla.ac.uk>

Aberration Corrected Lorentz Scanning Transmission Electron Microscopy

S. McVitie*, D. McGrouther, S. McFadzean, D. A. MacLaren, K. J. O'Shea and M. J. Benitez

Scottish Universities Physics Alliance, School of Physics and Astronomy, University of Glasgow, Glasgow, Glasgow G12 8QQ UK

Abstract

We present results from an aberration corrected scanning transmission electron microscope which has been customised for high resolution quantitative Lorentz microscopy with the sample located in a magnetic field free or low field environment. We discuss the innovations in microscope instrumentation and additional hardware that underpin the imaging improvements in resolution and detection with a focus on developments in differential phase contrast microscopy. Examples from materials possessing nanometre scale variations in magnetisation illustrate the potential for aberration corrected Lorentz imaging as a tool to further our understanding of magnetism on this lengthscale.

Keywords

Lorentz microscopy

Aberration correction

Magnetic thin films

Differential phase contrast

Corresponding author: stephen.mcvitie@glasgow.ac.uk

Introduction

The advent of aberration correction in the transmission electron microscope has led to a considerable increase in spatial resolution for both transmission electron microscopy (TEM) and scanning transmission electron microscopy (STEM) [i,ii]. Allied with improvements in electron sources that allow probes with an order of magnitude increase in current there are prospects for significant advances in our understanding of the functionality of advanced materials. Much of the effort in aberration corrected microscopy has been in the realm of imaging and spectroscopy at atomic resolution but there are also possibilities for advances in magnetic imaging in TEM/STEM which we showcase here.

Imaging of magnetic structure in TEM/STEM encompasses techniques that are collectively labelled Lorentz microscopy, spanning a range of qualitative and quantitative imaging methods including electron holography [iii]. In both Lorentz microscopy and holography the ultimate goal is recovery of the electron phase transmitted through the sample or related quantitative information. The basis for Lorentz imaging can be considered to be due to the classical Lorentz interaction arising from the component of magnetic induction perpendicular to the electron beam which results in a deflection of the beam. Films magnetised in-plane are therefore imaged easily whilst those with perpendicular magnetisation need to be tilted to produce a deflection. This angular deflection of the electron beam is known as β and for a saturated magnetic film, with saturation induction B_s and thickness t , we find that the maximum deflection is given by $\beta = e\lambda B_s t/h$. Here e is the magnitude of the electronic charge, λ is the wavelength of the electrons and h is Planck's constant. A typical value of deflection from 20 nm thick permalloy ($B_s = 1.0$ T) magnetised in-plane gives $12.7 \mu\text{rad}$. Alternatively Lorentz imaging may also be considered from a wave-optical quantum mechanical approach via the Aharonov-Bohm effect [iv]. The latter is required for a full explanation of the phase shifts that are measured by magnetic holographic imaging. Before considering the implications of aberration correction in the study of magnetic materials we firstly summarise the main magnetic imaging methods.

The most commonly used imaging mode in Lorentz TEM is the Fresnel mode [v] in which a defocused image reveals the position of domain walls. This mode is useful for identifying the geometry of magnetic domain structures and magnetisation reversal processes [vi,vii]. Generally large values of defocus are required due to the small Lorentz deflections and as such the resulting image contrast is not linearly related to the magnetic structure in the film. However applying the transport of intensity equation (TIE) [viii] to a series of defocused images can enable the phase of the electron wave to be reconstructed. In this case magnetic induction information may subsequently be calculated, as recently demonstrated for magnetic nanostructures [ix] and magnetic multilayer systems [x]. For quantitative interpretation of TIE phase reconstructions, particularly at high resolution, the defocus value used defines the extent to which the contrast can be considered linear. Any loss of high spatial frequency information will depend critically on the value of defocus used.

Aside from imaging, magnetic information may also be provided by the method of low (or small) angle diffraction in TEM. This is often used for characterisation of large areas of thin films but can also be used to gain information on nanostructured materials. The low angle diffraction pattern provides a measure of the Lorentz deflections across the illuminated area. However the deflection angles are usually of the order of a few tens of μrad , three orders of magnitude smaller than typical Bragg scattering angles. A large camera length (often hundreds of metres) is required to separate Lorentz deflected beams and gain quantitative information. This can be used to great effect, particularly for periodic magnetic structures, where the diffraction pattern has a contribution from the periodic structure and the magnetic domains [xi].

Apart from the TIE method quantitative imaging of magnetic structure in the TEM can be performed using electron holography and differential phase contrast. Electron holography is practised on a TEM and the phase information, reconstructed from holograms, can reveal quantitative information with great sensitivity. This method has been used for many magnetic studies to map induction in nanostructures and nanoparticles with phase noise sensitivity quoted up to $2\pi/250$ [xii,xiii]. Differential phase contrast (DPC) is practised on a STEM [xiv] and quantitatively images the magnetic induction. A quadrant detector is used and by taking difference signals from

opposite segments components of the deflection angle can be mapped which are equivalent to integrated in-plane components of induction. (The deflection angle quoted above, for a saturated film, is given more generally by $\beta = (e\lambda/h) \int Bdl$, where the integral is along the electron path dl). Many examples have been studied with this technique including patterned films with nanoconstrictions [xv] and multilayer magnetic films [xvi]. Furthermore the DPC method is also applicable for the study of in-plane electric fields [xvii]. An important consideration for Lorentz and holographic imaging of magnetic materials is that the majority of samples require low field or field free conditions at the specimen position. Therefore the objective lens of the microscope is usually switched off as detailed in the next section. In situ magnetising experiments may be carried out using the field from the weakly excited objective lens [xviii] or through special rods that can apply steady or pulsed fields [xix,xx].

Since the objective lens is no longer used for imaging the resolution in field free mode is determined by the lenses closest to the objective. Usually these lenses have a spherical aberration contribution of up to three orders of magnitude greater than the main objective lens (which have a spherical aberration constant, C_s , of only a few millimetres). In terms of aberration correction the in-focus direct imaging methods of holography and DPC stand to benefit most from improved resolution. The low angle diffraction method provides very sensitive spatial frequency information in diffraction space from a large sample area i.e. without high spatial resolution. Whilst the TIE method relies on defocused images it does have potential for benefit from aberration correction at very small defocus values where the loss of high spatial frequency information is limited.

As already stated, for Lorentz imaging of magnetic materials the sample is required to be located in a field free or low field environment. Therefore in an aberration corrected instrument the corrector needs to be adjusted to compensate not for the objective lens but for the alternative probe forming (STEM) or imaging (TEM) lens. Some preliminary reports have described tests and imaging carried out at 300 kV on aberration corrected instruments in field free or low field conditions in which the information limit is quoted as ~ 0.7 nm [xxi]. However mostly the reports concentrate

on Fresnel (i.e. defocused) based imaging including TIE reconstruction although the magnetic spatial variation within the presented images did not demonstrate the scale of the predicted resolution [xxii,xxiii,xxiv]. The improvements for the performance of holography, though not from a field free imaging perspective, have also been considered for aberration correction. An improved phase variation sensitivity of a factor of four has been reported in addition to the improvement in resolution [xxv].

In this paper we concentrate on the DPC mode of Lorentz STEM which provides quantitative induction maps and we demonstrate how aberration correction has allowed a significant improvement in resolution. This gives great potential for studies of a range of technological materials, in which being able to measure magnetic information on the nanometre length scale opens up the exploration of new areas of physics.

Experimental Set-up

The results reported in this paper were obtained from a JEOL Atomic Resolution Microscope (JEM-ARM200F), operating at 200 kV. The instrument is equipped with a cold field emission gun and a CEOS (Corrected Electron Optical Systems GmbH) corrector referred to as CESCOR that corrects for probe forming optics in STEM [xxvi]. A similar instrument equipped with a Schottky field emission gun reported atomic resolution in 2008 [xxvii] and advances in aberration correction have resulted in imaging with a sub 50 pm probe [xxviii]. The cold field emission source has enhanced brightness compared to Schottky emitters and has an energy spread down to 0.27 eV.

When the objective lens is used for standard imaging the sample sits in a field of ~ 2 T parallel to the optic axis of the microscope. Thus, for most magnetic samples, the magnetisation would be saturated in this direction. When the objective lens is switched off the sample experiences only the low remanent objective lens field, which is around 150 Oe for our instrument. (In our case we are able to reduce this field to < 1 Oe using field control hardware [xxix]). In practise the remanent field can be used to advantage, for samples with in-plane magnetisation. The out of plane demagnetising factor for thin films means that the remanent field is small enough not to seriously disturb the magnetic state with the sample in an untilted position [xxx].

However by then tilting the sample the introduction of an in-plane (sample) field component is used to change the magnetic state.

Previously in a non aberration corrected system [xviii] in STEM field free mode the condenser mini-lens is the image forming lens. The high spherical aberration of this lens (C_s is nearly 10 m compared to a few mm for the high resolution (HR) objective lens) limits the probe size to around 5 nm with a probe semiangle (α) of around 1 milliradian. Whilst this would offer the best resolution, the sensitivity of the DPC mode depends on the ratio of the Lorentz deflection angle (β) to α . For a 20 nm thick permalloy ($\text{Ni}_{80}\text{Fe}_{20}$) film $\beta \sim 12.7 \mu\text{rad}$ which is rather low in terms of sensitivity (β/α). Often this meant that a lower value of α was chosen to increase sensitivity albeit with a resulting loss of resolution.

In the present system with the cold field emission gun the source size gives only a very small contribution to the probe size and thus can be ignored [ii]. Therefore the probe size is limited only by diffraction and aberration contributions. Using the CESCOR to correct the probe forming lens the quality of the aberration correction is checked by observing the Ronchigram, the diffraction pattern in the detector plane. An example of a Ronchigram obtained under the optimum conditions for field free/low field probe formation is shown in Fig. 1 for a standard cross-grating test sample with 2160 lines per mm. In this case the Ronchigram possesses a flat region of a few milliradians in diameter due to the reduction of aberrations, principally the C_s value is reduced to the level of a few μm . This can be seen in Fig. 1 and the size of the flat region is indicated with a 70 μm radius condenser aperture size superimposed on the image by a red circle. In this mode this aperture then corresponds to $\alpha = 3.2 \text{ mrad}$. For a diffraction limited system the probe diameter is given by $1.22\lambda/\alpha$. Thus for an instrument with an accelerating voltage of 200 kV, giving $\lambda = 2.5 \text{ pm}$, the calculated probe diameter is $\sim 1 \text{ nm}$. The resolution defined, by the Rayleigh criterion is half of this value - i.e. 0.5 nm - which is in agreement with previous reports [xxi,xxii].

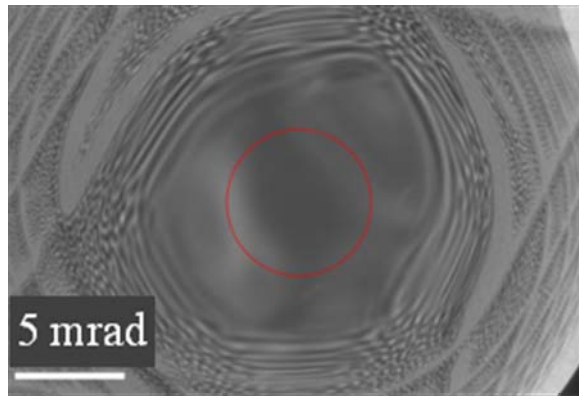


Fig. 1. Ronchigram of standard cross-grating sample (2160 line per mm) in field free (Lorentz) mode with the objective lens off and with the probe focused by the condenser mini lens. The red circle illustrates the extent of a 70 μm radius probe forming aperture.

Detection of the scanned electron probe after interaction with the specimen, has required extensive development of a multi-channel detector and a highly parallel acquisition setup. Our instrument is equipped with the commonly used STEM detectors including JEOL and Gatan bright field (BF), annular dark field (ADF) and high angle annular dark field (HAADF). Furthermore we also have a CFEG emission monitoring system. For DPC imaging we have mounted an 8-segment silicon photodiode array. The detector layout, optimised by us for high sensitivity DPC imaging [xiv], consists of a solid central quadrant surrounded by an outer annular quadrant and is mounted on a retractable mechanism located on-axis, below the main viewing screen (Deben UK Ltd.). Conversion of the charge current signals and further amplification are performed by a highly configurable 8-channel “Superfast” amplifier (Andrew Armit Designs / Deben UK Ltd.) capable of the output of individual or mixed video signals with a maximum bandwidth of 2MHz.

Acquisition of the 8 signals from the DPC system, in addition to our standard STEM has necessitated the incorporation of four Gatan “Digiscan II” units operating in parallel and providing capability to acquire and display up to 16 signals simultaneously. Overall control of the signal acquisition and live greyscale/colour display of magnetic induction (or other modes of differential phase contrast) has been achieved through a GUI script plug-in for Digital Micrograph software developed in-house with support from Gatan. Components of the magnetic induction are imaged by

taking difference signals from opposite segments of the detector mapping orthogonal components of the magnetic induction whilst the total signal falling on the detector is displayed as an equivalent BF image. One of the strengths of this system is that it allows simultaneous imaging of magnetic induction components and the physical structure by combining different signal combinations from the segmented detector.

Results

Initially the Lorentz imaging mode resolution was tested on a sample of evaporated gold nanoparticles which have a range of diameters down to around one nanometre. For the purpose of demonstrating the resolution the microscope was set up at 200 kV with the condenser mini-lens as the probe forming lens, the objective lens turned off and the CESCOR corrector active. A 70 μm diameter condenser aperture was used as the probe limiting aperture and images were collected via the high angle annular dark field (HAADF) detector. An image of these particles is shown in Fig. 2(a) and illustrate a range of nanoparticle sizes with shape being easily resolved around the nanometre scale. A small particle around 1 nanometre in size is indicated in the figure between the yellow arrows and the intensity linetrace shown in Fig. 2(b). The full width half maximum from this linetrace is shown to be 0.9 nm (the pixel size is 0.18 nm) showing that the nanometre sized particle is clearly resolved. Whilst extracting an exact figure from this variation is rather limited it is apparent the FWHM from Fig. 2(b) confirms the level of the resolution directly in an image. The data is consistent with a diffraction limited case for a 1 nanometre probe diameter and an associated Rayleigh resolution of around 0.5nm quoted above.

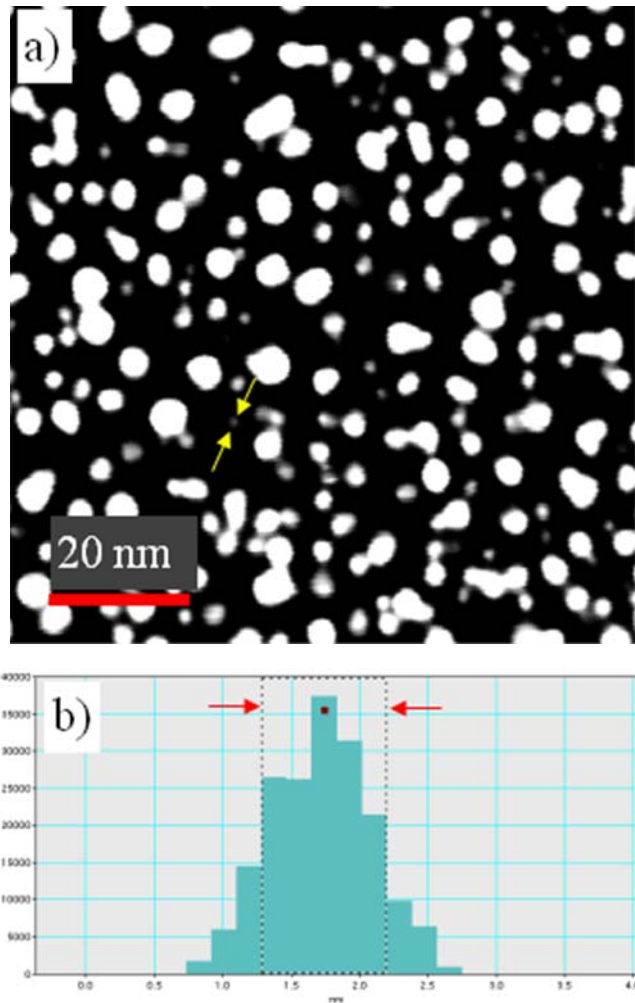


Fig. 2. a) HAADF image of gold nanoparticles in Lorentz STEM mode. b) Intensity linetrace taken along the line indicated by yellow arrows in a) from a single small nanoparticle, the distance between the red arrows in the linetrace is 0.9 nm.

We now present the first application of aberration corrected Lorentz STEM for two magnetic systems. Namely, i) “impure” iron nanoelements and ii) an exchange biased magnetic multilayer system. These systems are selected for their technological relevance and to demonstrate the importance of nanoscale magnetic imaging.

The first sample comprised ferromagnetic elements with side lengths from 50 – 500 nm fabricated using electron beam induced deposition (EBID) of Fe (from an $\text{Fe}(\text{CO})_6$ precursor gas) as described elsewhere [xxx]. The magnetic state of these low aspect ratio nanoelements displayed a flux closure structure and a pair of DPC images of a typical structure is shown in Figs. 3(a) and (b). These DPC induction maps indicate

that the element possesses a double vortex closure structure, which can be strikingly represented in a false colour map shown in Fig. 3(c). The colour map displays in-plane induction directions corresponding to the small colour wheel key inset with bright/dark colour contrast indicating the magnitude and direction of the magnetic induction. Although this material is not pure iron the vortex core diameter should be on the order of the exchange length. This length is calculated from material parameters and given by $\sqrt{A/\mu_o M_s^2}$ where A is the exchange constant, μ_o the permeability of free space and M_s the saturation induction of the material. For pure iron the exchange length is 1.5 nm, whilst for a soft material like permalloy it is 4 nm. The vortex core size has previously been measured for permalloy to be around twice the exchange length [xxxii]. It is likely that the EBID deposit has a composition close to Fe(60%)O(30%)C(10%) [xxxi] and accordingly the element displays a flux closure structure suggesting that the material is indeed quite soft. The extent of the vortex core is measured by taking a single linetrace across the centre of the vortex from either of the induction maps, displayed as a quantitative deflection angle, which is shown in Fig. 3(d). Note that the deflection angle is proportional to the integrated induction, the maximum deflection values in each domain here is $\pm 25 \mu\text{rad}$. This corresponds to an integrated induction of $\pm 40 \text{ T nm}$. For a film of thickness 100 nm this corresponds to a saturation induction of $\sim 0.4 \text{ T}$ which equates to a saturation magnetisation of around 350 kA m^{-1} . Whilst there is some residual signal variation, mainly due to the substrate, the tight spatial variation of the induction is clearly visible and indicates a vortex core size of around 13 nm. In simple terms this value is consistent with the Fe content of the deposited film being considerably lower than pure iron (reported as $\sim 60\%$ of that for pure Fe in [xxxii] for the EBID sample).

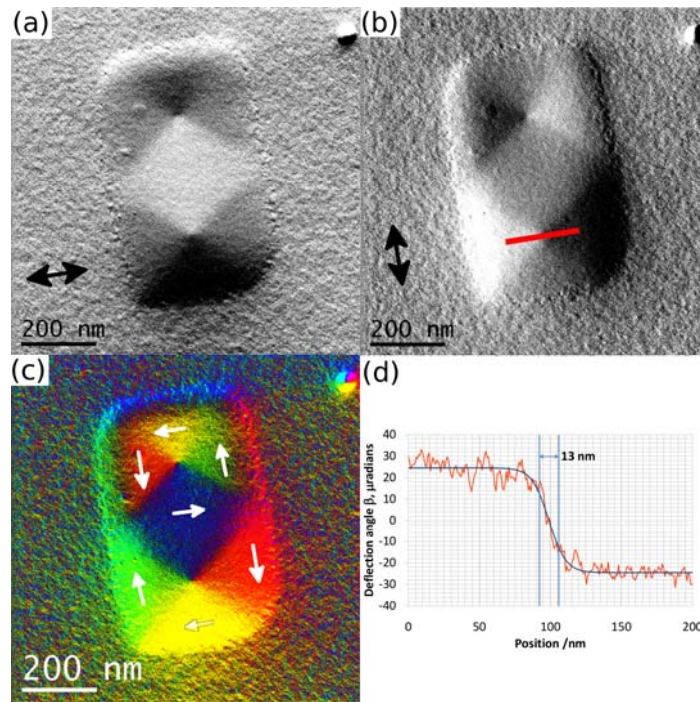


Fig. 3. a) and b) Gray scale images of an electron beam induced fabricated nanostructure of FeCO showing mapping of the integrated in-plane induction components as indicated by the double headed arrows. c) Colour representation of the DPC images with colour wheel (inset top right). d) Linetrace from image b) showing the induction profile, as a measured deflection angle in microradians, at the vortex core.

The second sample was an exchange biased sputtered sample comprising a multilayer structure of ferromagnetic NiFe layers between anti-ferromagnetic FeMn layers with the structure NiFe/(FeMn/NiFe) \times 10 grown on an oxidised Si substrate with a capping layer of 5nm of Ta. The NiFe layers had an average thickness of 16.5 nm and the FeMn layers an average of 12.8 nm, measured from high resolution STEM. The samples were grown at Queens University Belfast in their UHV co-sputtering system [xxxiii]. To demonstrate the magnetic capability of the microscope a cross-section sample was prepared using focused ion beam methods resulting in a section which was \sim 80 nm thick. The exchange bias coupling between the AF and FM layers shows hysteretic behaviour in the continuous film sample with the individual layers reversing in steps so that the sample reversed completely in a field of \sim 150 Oe. However in the case of the cross-section the sectioning has in effect patterned each FM layer into a nanowire geometry and the fields required to reverse each layer were

much higher. Using the ARM with CESCOR it was possible to image the state of each layer and map induction changes by using the objective lens field and tilting to reverse the magnetic state of the layers. Initially the sample was immersed in a large field (around 1000 Oe) to set all the layers in parallel alignment. The DPC image component showing the magnetic induction parallel to the interfaces is shown in Fig. 4(a) where the ferromagnetic NiFe layers appear as bright stripes in the image and the FeMn layers are gray indicating no net induction component in these regions. The arrows at the top of the image indicate the direction of magnetization in each ferromagnetic layer. The variation in contrast within the stripes is a consequence of the granular structure of the film and this gives rise to a diffraction contribution in the phase contrast image. A linetrace from the area indicated by the red rectangle in Fig 4(a) is shown below the image, which averages the signal over a 40 nm width to reduce the effects of diffraction contrast from the granular structure. The linetrace is shown quantitatively as a deflection angle in microradians, noting that 50 μrad corresponds to an integrated induction of 80 T nm. Thus for a ~ 80 nm thick cross-section this is consistent with a saturation induction of the permalloy of 1.0 T. However it should be noted that there is significant amount of non-magnetic contrast from the grain structure and focused ion beam damage from the cross-section fabrication to cause variations in the signal observed in the trace and images. The profile shows the magnetised layer variation where each magnetic layer is around 16-17 nm wide (i.e. the thickness of the deposited film) and the AF layer is 13 nm wide. By tilting the sample in the objective lens field the magnetic state was altered: individual layers switch and an example of the state part-way through the reversal process is shown in Fig. 4(b). Here seven of the eleven magnetic layers have switched their direction of magnetisation and now appear dark, with one partially switched as indicated by the arrows above the image. The linetrace below the image shows the deflection/induction in the ferromagnetic layers very clearly and indeed the transition between the FM and AF layers shows a variation on the order of 5 nm.

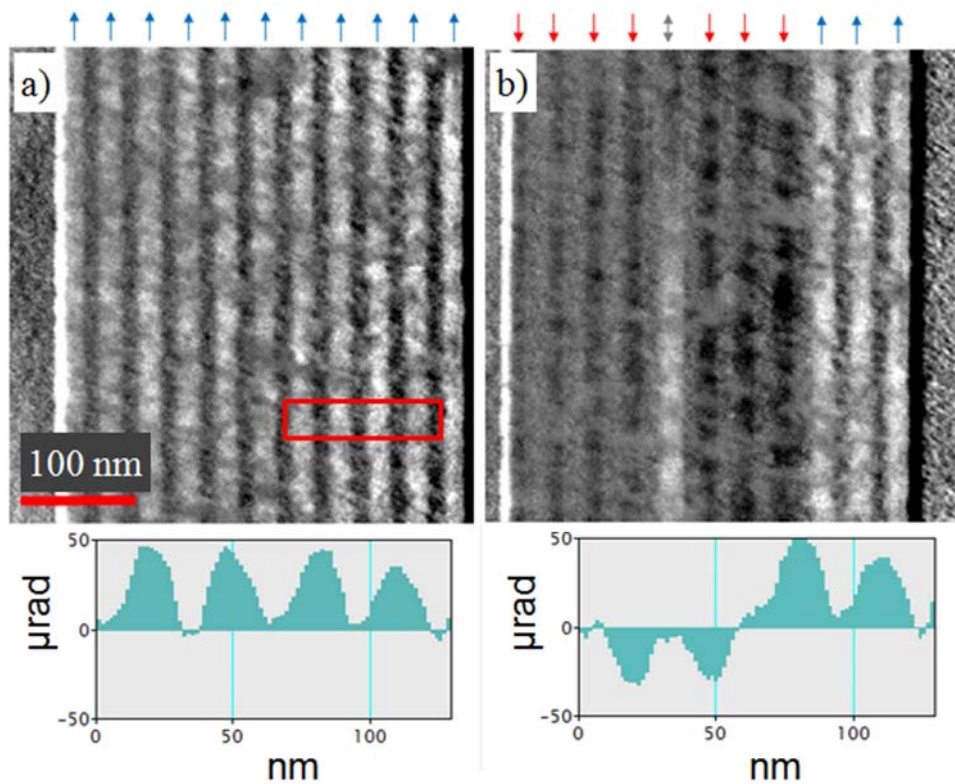


Fig. 4. DPC images and lineprofiles of a cross-section of an exchange biased multilayer structure NiFe(20nm)/[FeMn(15nm)/NiFe(20nm)] \times 10/Ta. The images are sensitive to the induction component along the interfaces and show the sample a) after a saturating field and b) during a field reversal. The arrows at the top indicate the direction of magnetization in each magnetic layer. Lineprofiles are shown below each image of the induction variation as a quantitatively measured deflection angle in microradians, taken from the region of the red box in a).

Conclusion

We have demonstrated the capability of a probe corrected STEM instrument for Lorentz DPC imaging that can provide quantitative induction maps with a spatial resolution around one nanometre. This instrument opens up exciting possibilities for imaging new and existing materials with imaging resolution below the exchange length for many materials. However measuring samples possessing a low intrinsic

moment or which are very thin remains a challenge due to the resulting small Lorentz deflection angles - particularly in the presence of diffraction effects. In respect of the latter we are also progressing detection methods and currently exploring possibilities using a pixelated detector where an image of the diffraction disk is acquired at each point of the scan and the image processed to reduce the diffraction contribution to the DPC image. We expect to report such developments in the near future.

Acknowledgements

We would like to thank colleagues at JEOL, JEOL (UK), Gatan, Deben UK Ltd. and Andrew Armit Designs for their input to the development of the instrument. Furthermore we thank colleagues at the Technical University of Eindhoven for provision of the EBID sample. Additionally we are grateful to Prof R. Bowman and Dr S. O'Reilly of Queen's University Belfast for provision of the exchange biased sample and to Mr F. Gonclaves and Mr W. Smith for preparation of the cross-sectional sample. We also acknowledge financial support from the Scottish Universities Physics Alliance (SUPA), the University of Glasgow and Seagate.

-
- ⁱ M. Haider, H. Rose, S. Uhlemann, B. Kabius, K. Urban, J. Electron Microscopy, 47 (1998) 395.
- ⁱⁱ O.L. Krivanek, G.J. Corbin, N. Dellby, B.F. Elston, R.J. Keyse, M.F. Murfitt, C.S. Own, Z.S. Szilagy, J.W. Woodruff, 108 (2008) 179–195.
- ⁱⁱⁱ J.N. Chapman and M. R. Scheinfein, J. Magn. Magn Mater., 200 (1999) 729-740.
- ^{iv} Y. Aharonov and D. Bohm, Phys. Rev 115 (1959) 485.
- ^v S. McVitie, M. Cushley, Ultramicroscopy 106 (2006) 423.
- ^{vi} D. Petit, H. T. Zeng, J. Sampaio, E. R. Lewis, L. O'Brien, A.-V. Jausovec, D. E. Read, R. P. Cowburn, K. J. O'Shea, S. McVitie, and J. N. Chapman, Appl. Phys. Lett. 97 (2010) 233102.
- ^{vii} T. Uhlig, M. Rahm, C. Dietrich, R. Hollinger, M. Heumann, D. Weiss, and J. Zweck, Phys. Rev. Lett. 95 (2005) 237205.
- ^{viii} D. Paganin and K. A. Nugent, Phys. Rev. Lett., 80 (1998) 2586-2589.
- ^{ix} S. Bajt, A. Barty, K.A. Nugent, M. McCartney, M. Wall, D. Paganin, Ultramicroscopy, 83 (2000) 67–73.
- ^x C. Phatak, A. K. Petford-Long, and O. Heinonen, Phys. Rev. Lett. 108 (2012) 067205.
- ^{xi} Y. Togawa, T. Koyama, K. Takayanagi, S. Mori, A. Kousaka, J. Akimitsu, S. Nishihara, K. Inoue, A. S. Ovchinnikov, and J. I. Kishine, Phys. Rev. Lett. 108 (2012) 107202.
- ^{xii} A. Tonomura, Adv.Phys. 41 (1992) 59–103.
- ^{xiii} R. P. G. McNeil, R. J. Schneble, M. Kataoka, C. J. B. Ford, T. Kasama, R. E. Dunin-Borkowski, J. M. Feinberg, R. J. Harrison, C. H. W. Barnes, D. H. Y. Tse, T. Trypiniotis, J. A. C. Bland, D. Anderson, G. A. C. Jones, and M. Pepper, Nano Lett. 10 (2010) 1549.
- ^{xiv} J. N. Chapman, I. R. McFadyen, and S. McVitie, IEEE Trans. Magn. 26 (1990) 1506.
- ^{xv} M. C. Hickey, D-T. Ngo, S. Lepadatu, D. Atkinson, D. McGrouther, S. McVitie and C.H. Marrows, Appl. Phys. Lett. 97 (2010) 202505.
- ^{xvi} X. Kong, S. McVitie, J. N. Chapman, J. M. R. Weaver, D. O. O'Donnell and A. B. Johnston, J. Appl. Phys., 104 (2008) 013925.

-
- xvii M. Lohr, R. Schregle, M. Jetter, C. Wächter, T. Wunderer, F. Scholz, J. Zweck, *Ultramicroscopy*, 117 (2012) 7–14.
- xviii S. McVitie and J. N. Chapman, *Microsc. Microanal.*, 3 (1997) 146-153.
- xix A. Budruk, C. Phatak, A.K. Petford-Long, M. De Graef, *Acta Mater*, 59 (2011) 4895–4906.
- xx G. Yi, W. A. P. Nicholson, C. K. Lim, J. N. Chapman, S. McVitie, C. D. W. Wilkinson, *Ultramicroscopy*, 99 (2004) 65-72.
- xxi B. Freitag, M. Bischoff, H. Mueller, P. Hartel, and H. V. Harrach, *Microsc. Microanal.*, 15 (2009) 184.
- xxii R. Dunin-Borkowski, L. Houben, J. Barthel, A. Thust, M. Luysberg, B. B. Chris, K. András, T. Kasama, R. J. Harrison and J. R. Jinschek, *Microsc. Microanal.*, 18 (2012) 1708 – 1709.
- xxiii N. T. Nuhfer, A. Budruk and M. De Graef, *Microsc. Microanal.*, 16 (2010) 142–143.
- xxiv C. Phatak, J. A. Bain, J. G. Zhu and M. De Graef, *Microsc. Microanal.* 14 (2008) 832 – 833.
- xxv D. Geiger, H. Lichte, M. Linck, M. Lehmann, *Microsc. Microanal.* 14 (2008) 68-81.
- xxvi M. Haider, S. Uhlemann, and J. Zach, *Ultramicroscopy* 81(2000) 163–175.
- xxvii R. F. Klie, C. Johnson and Y. Zhu, *Microsc. Microanal.* 14 (2008) 104 – 112.
- xxviii R. Erni, M. D. Rossell, C. Kisielowski, and U. Dahmen, *Phys. Rev. Lett.*, 102 (2009) 096101.
- xxix A. Kohn and A. Habibi, *JEOL News*, 47 (2012) 22.
- xxx K. J. Kirk, J. N. Chapman, S. McVitie, P. R. Aitchison, C. D. W. Wilkinson, *Appl Phys Lett*, 75 (1999) 3683-3685.
- xxxi R. Lavrijsen, R. Cordoba, F. J. Schoenaker, T. H. Ellis, B. Barcones, J. T. Kohlepp, H. J. M. Swagten, B. Koopmans, J. M. De Teresa, C. Magen, M. R. Ibarra, P. Trompenaars, J. J. L. Mulders, *Nanotechnology* 22 (2011) 025302.
- xxxii X. Liu, J. N. Chapman, S. McVitie, C. Wilkinson, *Appl Phys Lett*, 84 (2004) 4406 – 4408.
- xxxiii C. B. Hill, W. R. Hendren, R. M. Bowman, P. K. McGeehin, M. A. Gubbins and V. A. Venugopal, *Meas. Sci. Technol.*, 24 (2013) 045601.
